

DYNAMO ACTION DUE TO EKMAN LAYER INSTABILITY

YANNICK PONTY

*Observatoire de la Côte d'Azur, Laboratory Cassini -
CNRS UMR 6529, B. P. 4229, 06304 Nice Cedex 4, France*

AND

ANDREW GILBERT AND ANDREW SOWARD

*School of Mathematical Sciences, University of Exeter,
North Park Road, Exeter, Devon EX4 4QE, UK*

1. Introduction

The Ekman layer becomes hydrodynamically unstable at sufficiently large Reynolds number Re . For the case of purely vertical rotation, the Ekman layer instability has been studied experimentally by Faller [4] and Caldwell & Van Atta [1], and numerically by Faller & Kaylor [5], Lilly [10], Melander [11] and Ponty *et al.* [13]. The linear and nonlinear behaviour of Ekman–Couette instabilities in a plane layer has been discussed by Hoffmann *et al.* [8]. The transition between the Taylor–Couette instability and the Ekman layer instability is explored in Hoffmann & Busse [9]. Two different Ekman layer instabilities are distinguished in these studies, which for historical reasons are now referred to as types I and II. Type II occurs when the Reynolds number Re^* defined using the Ekman layer thickness, exceeds the experimentally measured value of $Re_c^* \simeq 56.7$ (or 124.5 for type I). We will focus on the type II travelling wave, which has the smaller critical Reynolds number and so is easier to study numerically.

We simulated the finite amplitude development of the Ekman instability with our nonlinear numerical code subject to two-dimensional restrictions. Within that framework, we reach Reynolds numbers (based on the depth of the layer) of up to 800 and find that the saturated flow remains steady in a moving frame. Since such flow has no chaotic particle paths, any resulting dynamo cannot be fast. Nevertheless, we have found robust slow dynamo action which we now discuss.

2. Governing equations

2.1. DIMENSIONLESS EQUATIONS

We consider a Cartesian fluid layer of depth h , rotating with angular velocity $\mathbf{\Omega} = \Omega \hat{\mathbf{\Omega}} = \Omega(\cos \vartheta \hat{\mathbf{z}} + \sin \vartheta \hat{\mathbf{y}})$ ($\Omega \geq 0$), which models a thin shell locally at co-latitude ϑ ($\hat{\mathbf{x}}$ East; $\hat{\mathbf{y}}$ North; $\hat{\mathbf{z}}$ vertical). The top and bottom boundaries are rigid; the top boundary is fixed, while the bottom moves with velocity $\mathbf{U}_0 = U_0 \hat{\mathbf{x}}$. The fluid has viscosity ν and magnetic diffusivity η . Length, time and velocity are non-dimensionalised using the depth h and the viscous time-scale h^2/ν . After non-dimensionalisation, the velocity at the bottom boundary becomes $\mathbf{U} = (U_0 h/\nu) \hat{\mathbf{x}} = Re \hat{\mathbf{x}}$; the basic steady, non-magnetic, equilibrium state depends only on the vertical coordinate z . The absence of an imposed horizontal pressure gradient ensures that the bulk of the basic horizontal shear $Re \mathbf{\Lambda}(z)$ driven by the differential motion of the plane parallel boundaries is concentrated in an Ekman layer attached to the bottom boundary. We calculate the Ekman profile $\mathbf{\Lambda}(z)$ analytically and note that the Ekman boundary layer thickness is $1/\sqrt{\tau} \cos \vartheta$.

Once the steady shear is disturbed, we write $\mathbf{U} = Re \mathbf{\Lambda}(z) + \mathbf{u}$. We assume spatial periodicity in the unbounded horizontal direction. The magnetic field \mathbf{B} is taken to obey insulating boundary conditions. Accordingly the no-slip boundary conditions imply that $\mathbf{u} = 0$ on $z = 0$ and 1. The governing equation become

$$\begin{aligned} \partial_t \mathbf{u} + \mathbf{u} \cdot \nabla \mathbf{u} + Re(\mathbf{\Lambda} \cdot \nabla \mathbf{u} + u_z \partial_z \mathbf{\Lambda}) + \tau \hat{\mathbf{\Omega}} \times \mathbf{u} &= -\nabla \Pi + \nabla^2 \mathbf{u} + (\nabla \times \mathbf{B}) \times \mathbf{B}, \\ \partial_t \mathbf{B} + \mathbf{u} \cdot \nabla \mathbf{B} - \mathbf{B} \cdot \nabla \mathbf{u} + Re(\mathbf{\Lambda} \cdot \nabla \mathbf{B} - B_z \partial_z \mathbf{\Lambda}) &= P_m^{-1} \nabla^2 \mathbf{B}. \end{aligned}$$

The dimensionless parameters employed are

$$\tau = 2\Omega h^2/\nu, \quad P_m = \eta/\nu, \quad Re = U_0 h/\nu,$$

namely the square root of Taylor number, the magnetic Prandtl number and the Reynolds number respectively. With a suitable choice of units for the magnetic field, we avoid the introduction of any additional coefficient in a front of the Lorenz force term.

2.2. TWO-DIMENSIONAL FORMULATION

At the onset of fluid instability, the fluid motion takes the form of rolls with a specific orientation. This flow is two-dimensional independent of the coordinate \bar{y} along the roll axes. Our main assumption is that the two-dimensionality at onset is maintained in the fully developed nonlinear state, so that the velocity has the restricted functional form $\mathbf{u}(\bar{x}, z, t)$, where \bar{x} is the horizontal coordinate normal to the roll axis.

To investigate the possibility of dynamo action in our \bar{y} -independent fluid flow, we consider magnetic field described by \bar{y} -dependent normal modes of the form $\mathbf{B} = \mathbf{b}(\bar{x}, z, t) \exp(il\bar{y})$ ($l \neq 0$). The Lorenz force is projected on the zero- l mode of the momentum equation by taking into account only the beating of conjugate magnetic modes $l = \pm 1$. Our simplifying two-dimensional assumption is important because it allows us to study dynamo action at large magnetic Reynolds number with high numerical resolution.

Since \mathbf{u} is independent of \bar{y} , we may write $\mathbf{u} = -\partial_z \psi \hat{\mathbf{x}} + v \hat{\mathbf{y}} + \partial_{\bar{x}} \psi \hat{\mathbf{z}} = \nabla \times (\psi \hat{\mathbf{y}}) + v \hat{\mathbf{y}}$. Furthermore, since the flow is steady in a frame co-moving with the rolls, it is helpful to define the total stream function

$$\Psi(\bar{x}, z) = \psi(\bar{x}, z) - Re P \int_0^z \Lambda(\xi) \cdot \hat{x} d\xi + U_{\text{roll}} z.$$

In that moving frame (relative velocity U_{roll}), partricles follow the stream lines $\Psi = \text{constant}$ and the components of the total velocity are

$$U - U_{\text{roll}} = -\partial_z \Psi, \quad V(\bar{x}, z) = v(\bar{x}, z) + Re P \Lambda(z) \cdot \hat{y}, \quad W = \partial_{\bar{x}} \Psi.$$

3. Numerical method and diagnostics

The solution of the magnetohydrodynamic system is achieved numerically using a time-stepping pseudo-spectral code with the collocation-tau method (see Ponty *et al.* [14] for further details).

The results of our simulations, especially from the kinematic dynamo viewpoint, depend on the magnetic Reynolds number Rm . Thus we introduce the root-mean-square value \mathcal{U} of the non-dimensional total velocity \mathbf{U} , averaged over both space and time, and define $Rm = P_m \mathcal{U}$. We also introduce turn-over time-scale $\lambda = \sigma/\mathcal{U}$ measured by the real magnetic field growth rate σ based on the viscous time scale.

4. Fluid topology

We present one example of dynamo in flows resulting from the Ekman instability. We take $\vartheta = 67.5^\circ$, $\tau = 100$ and $k_c = 4.30$; our Reynolds number is $Re = 250$, which is to be compared to the critical value $Re_c \simeq 138$ for the instability. The results are illustrated in figures 1(a,b), which give the \bar{y} -velocity V and total stream function Ψ in the co-moving frame. The stream lines of the ensuing finite amplitude flow have the cats' eye configuration, which is well known to occur at critical levels in other shear flows, e.g., the Kelvin–Helmholtz instability. In the (\bar{x}, z) -plane, this stream line topology contains elliptic and hyperbolic stagnation points. The exponential stretching at the stagnation points, and the differential rotation around the elliptic points can stretch out field, contributing to a dynamo process.

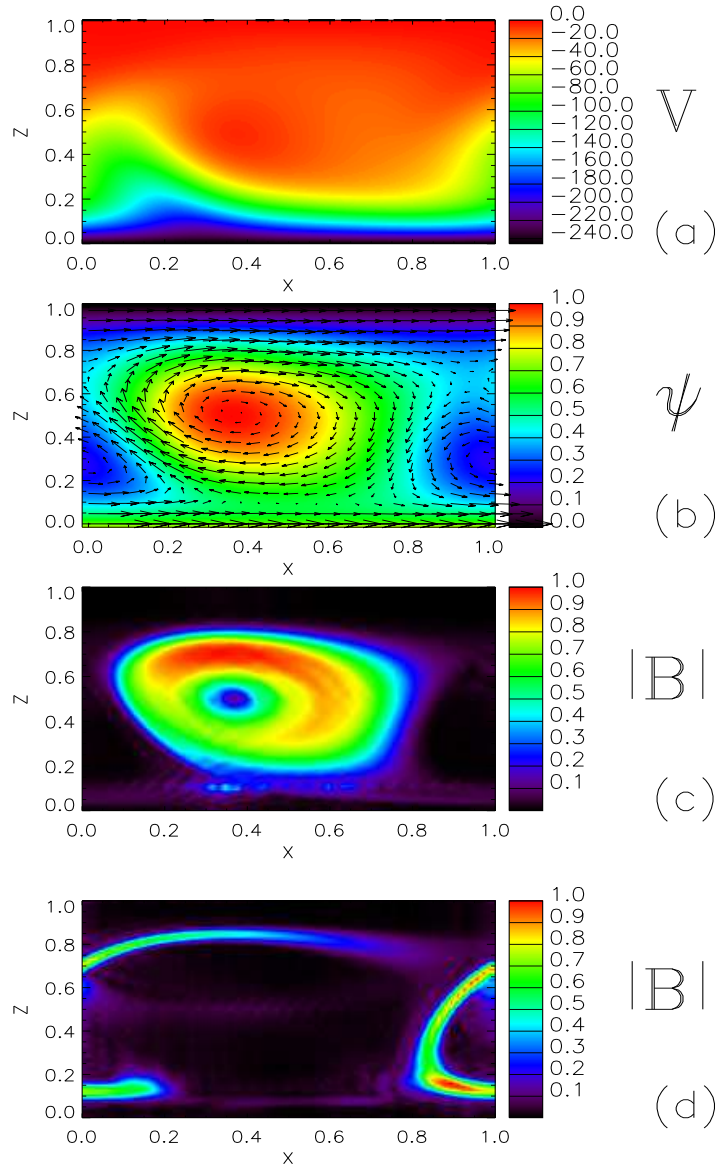


Figure 1. A flow resulting from a saturated Ekman layer instability drives a dynamo for $\vartheta = 67.5^\circ$, $\tau = 100$, $\epsilon = 79.28^\circ$, $k_c = 4.64$, $Re = 250$ and $P_m = 40$, corresponding to $Rm \simeq 3600$. It is shown a as time-snapshot in the (\bar{x}, z) plane of (a) the total velocity V along the \bar{y} -axis, (b) the total stream function Ψ , (c) the magnitude B of the magnetic field in the case $l = 1.2$, and (d) the magnitude B of the magnetic field in the case $l = 9.0$.

5. Kinematic dynamo

Different kinematic dynamo mechanisms are found, which largely depend on the size of the wave number l . Figure 2 shows the growth rates σ and λ plotted against the wave number l for $P_m = 40$, when $Rm \simeq 3600$. The curve is complicated, having many peaks and windows of dynamo and non-dynamo action as l is varied.

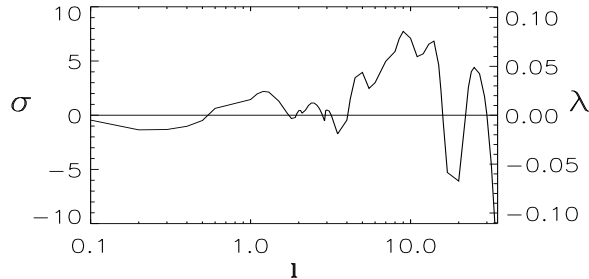


Figure 2. The magnetic field growth rate plotted against the wave number l along the \bar{y} axis, with two scalings: σ on the left-hand side is scaled with the thermal diffusion time, and λ on the right-hand side with the turn-over time. The flow is an equilibrated Ekman layer instability with parameters as in figure 1.

Below the wave number $l \simeq 2.0$, the magnetic field shown in figure 1(c) for $l = 1.2$ is concentrated around the principal vortices of the flow displayed in figure 1(b). The dynamo process appears to correspond to the Ponomarenko dynamo [12] (see Gilbert [6], Ruzmaikin, Sokoloff & Shukurov [16], Gilbert & Ponty [7]). Field directed in or out of the eddy is stretched by differential rotation on helical streamlines to generate field directed along the streamlines. Diffusion of this field in curved geometry generates field across streamlines so closing the dynamo loop and leading to magnetic field amplification. To confirm this picture, the magnetic field, which takes the form of two spiralling tubes, is visualised in three dimensions in figure 3.

Above the wave number $l \simeq 2.0$, the magnetic field is localised along the separatrices and the stagnation points play a crucial role. The magnitude of the magnetic field is shown in figure 1(d) for $l = 9.0$, where the magnetic growth rate is a maximum in the figure 2. We see that the dominant magnetic mode has field localised in sheets along the separatrices of the flow in the (\bar{x}, z) -plane (using the stream function Ψ for the appropriate moving frame). The sheets intersect at the hyperbolic stagnation points. Our simulation represents the first example of a dynamo effect obtained in a cats' eyes configuration resulting from hydrodynamic instability.

The dynamo mechanism, just described, has some similarities with that of the periodic G.O Roberts [15] cellular flow investigated analytically in the

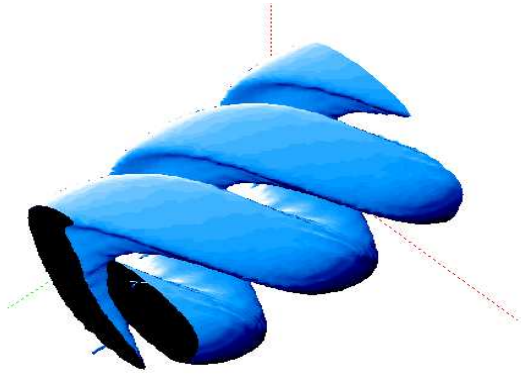


Figure 3. A three dimensional visualisation of the magnetic field in the case shown in figure 4(c). An iso-surface of constant magnitude of magnetic field is plotted with respect to (\bar{x}, \bar{y}, z) axes.

large- Rm limit by Childress [2] and Soward [17]. In this case the field is also associated with the stagnation points and separatrices, and is amplified by a steady stretch–fold–shear mechanism. Dynamo action is also considered for doubly periodic rows of cats’ eyes by Childress & Soward [3], who compute an α –effect associated with boundary layers on the separatrices. Their calculations involve averaging over the infinite plane, and it remains to be seen how their results relate to dynamo action in our row of cats’ eyes in a plane layer with insulating boundaries.

In our example of a saturated Ekman instability, we have identified two different kinematic dynamo mechanisms which compete with each other. The stretch–fold–shear mechanism in the steady flow is the more efficient one, preferring modes with short scale in the \bar{y} direction, but the Ponomarenko mechanism is also there, subdominant, preferring large-scale fields. Note that regardless of the wavenumber l in the \bar{y} -direction the two mechanisms tend to amplify fields of different length-scales in the (\bar{x}, z) -plane for large Rm , as seen in figure 1(c,d). For $l = O(1)$ the Ponomarenko dynamo amplifies field on $O(Rm^{-1/4})$ length-scales (Gilbert & Ponty [7]), while the fields associated with the hyperbolic stagnation points localise on $O(Rm^{-1/2})$ length-scales (Childress [2]) – harder to resolve numerically.

6. Nonlinear regime

Solutions in the fully nonlinear regime have been computed. In figure 4 the magnetic energy and the kinetic energy are plotted versus time for a particular set of parameter values. In figure 4a, the initial linear kinematic regime is clearly distinguished from the subsequent nonlinear saturation. The magnetic energy and the kinetic energy appear to settle down to steady values

but with slowly decaying transient oscillations. Throughout the range of wave number l displayed in figure 2, the system converges to the same kind of magnetohydrodynamic solution; here the saturated magnetic field is located around the separatrices, just as in large wave number kinematic case (see figure 1d). It means that a short magnetic length scale along the roll \bar{y} axis is then preferred.

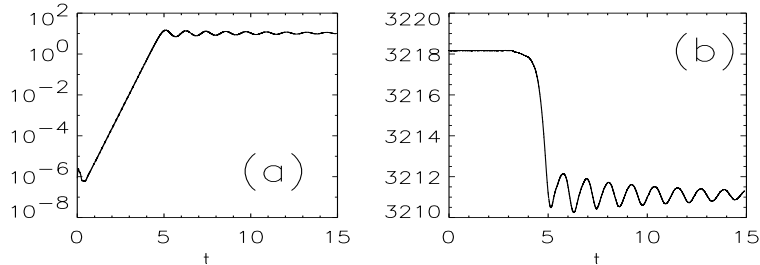


Figure 4. (a) The magnetic energy is plotted in log scale versus the running time for the same parameter values as in figure 1. (b) The kinetic fluid velocity associated is also presented.

7. Discussion

The equilibrated Ekman layer instability flows have the cats' eyes configuration and are steady in a co-moving frame. Here kinematic dynamo action may occur by the Ponomarenko [12] dynamo mechanism or with fields associated with hyperbolic stagnation points and their connecting separatrices. The Ponomarenko mechanism is now well-understood: asymptotic high- Rm growth rates may be obtained in cases such as those seen in the simulations with an arbitrary flow profile (Gilbert & Ponty [7]).

Kinematic dynamo action associated with hyperbolic stagnation points and separatrices is rather more complicated. Though dynamo action in flows with cats' eyes in the doubly-periodic plane has been studied by Childress & Soward [3], there are non-trivial geometrical complications that arise in the flows of our plane layer model. In particular the layer is periodic in only one direction, along the cats' eyes, and the velocity perpendicular to the plane of the cats' eyes is not constant on stream lines. It remains an interesting asymptotic problem to obtain high- Rm growth rates in this more general situation.

In the nonlinear regime, a stable nonlinear saturation is preferred, with the magnetic field located along the cats' eyes separatrices. Interestingly, the feed back of the Lorentz force does not appear to destroy the separatrix topology, which leads to an efficient kinematic dynamo process. Perhaps these features render the steady equilibrium robust.

In conclusion, dynamo action due to the Ekman layer instability provides a nice magnetohydrodynamic system for analytic study. Indeed we intend to undertake further detailed investigations of kinematic growth rates and the nonlinear equilibrium in ongoing studies.

Acknowledgments

Y.P. gratefully acknowledges the support of a Leverhulme Fellowship, grant no. F/144/AH, at the University of Exeter between August, 1997 and August, 2000. The numerical calculations were performed using the computing facilities of the laboratory Cassini, Observatoire de la Côte d’Azur (France), provided by the program “(SIVAM)” and the computing facilities of the parallel computer Ceres at the University of Exeter.

References

1. Caldwell, D.R. & Van Atta, C.W. 1970 Characteristics of Ekman boundary layer instabilities. *J. Fluid Mech.* **44**, 79–95.
2. Childress, S. 1979 Alpha-effect in flux ropes and sheets. *Phys. Earth Planet. Int.* **20**, 172–180.
3. Childress, S. & Soward, A.M. 1989 Scalar transport and alpha-effect for a family of cat’s-eyes flows. *J. Fluid Mech.* **205**, 99–133.
4. Faller, A.J. 1963 An experimental study of the instability of the laminar Ekman boundary layer. *J. Fluid Mech.* **15**, 560–576.
5. Faller, A.J. & Kaylor, R.E. 1966 A numerical study of the instability of laminar Ekman boundary layer flow. *J. Atmos. Sci.* **23**, 466–480.
6. Gilbert, A.D. 1988 Fast dynamo action in the Ponomarenko dynamo *Geophys. Astrophys. Fluid Dynam.* **44**, 241–258.
7. Gilbert, A.D. & Ponty, Y. 2000 Slow Ponomarenko dynamos on stream surfaces. *Geophys. Astrophys. Fluid Dynam.*, in press.
8. Hoffmann, N.P., Busse, F.H. & Chen, W.-L. (1998) Transition to complex flows in the Ekman–Couette layer. *J. Fluid Mech.* **366**, 311–331.
9. Hoffmann, N.P. & Busse, F.H. (1999) Instabilities of shear flows between two coaxial differentially rotating cones. *Phys. Fluids* **11**, 1676–1678.
10. Lilly, D.K. (1966) On the instability of Ekman boundary flow. *J. Atmos. Sci.* **23**, 481–494.
11. Melander, M.V. (1983) An algorithmic approach to the linear stability of the Ekman layer. *J. Fluid Mech.* **132**, 283–293.
12. Ponomarenko, Y.B. (1973) On the theory of hydromagnetic dynamos *Zh. Prikl. Mekh. & Tekh. Fiz.* **6**, 47–51.
13. Ponty, Y., Gilbert, A.D. & Soward, A.M. (2000) Rotating convective instability in an Ekman layer driven by a shear flow. in preparation.
14. Ponty, Y., Gilbert, A.D. & Soward, A.M. (2000) Kinematic dynamo in large magnetic Reynolds number flows driven by shear and convection *J. Fluid Mech.*, submitted.
15. Roberts, G.O. (1972) Dynamo action of fluid motions with two-dimensional periodicity. *Phil. Trans. R. Soc. Lond. A* **271**, 411–454.
16. Ruzmaikin, A.A., Sokoloff, D.D. & Shukurov, A.M. (1988) A hydromagnetic screw dynamo. *J. Fluid Mech.* **197**, 39–56.
17. Soward, A.M. (1987) Fast dynamo action in a steady flow. *J. Fluid Mech.* **180**, 267–295.